# Insights into Microstructural Features Governing $Ce^{3+}$ Luminescence Efficiency in Sol−Gel Silica Glasses

A. Vedda,*,† N. Chiodini,† D. Di Martino,† M. Fasoli,† F. Morazzoni,† F. Moretti,† R. Scotti,† G. Spinolo,† A. Baraldi,‡ R. Capelletti,‡ M. Mazzera,‡ and M. Nikl§

*Department of Materials Science, INSTM and CNISM, University of Milano−Bicocca, Via R. Cozzi 53, 20125 Milano, Italy, Department of Physics and CNISM, University of Parma, Viale G.P. Usberti 7/A Campus Universitario, 43100 Parma, Italy, and Institute of Physics, Academy of Sciences of the Czech Republic, Cukrovarnicka 10, 162 53 Prague, Czech Republic*

*Received July 27, 2006. Revised Manuscript Received October 4, 2006*

The radioluminescence (RL) properties of Ce-doped silica glasses prepared by sol−gel method were investigated as a function of the dopant amount in a wide range of concentrations (Ce:Si molar ratios from $1 \times 10^{-5}$ to $5 \times 10^{-2}$). The effects of xerogel densification temperature and of a postdensification thermal treatment were also considered. In order to understand the microstructural features governing $Ce^{3+}$ luminescence efficiency, optical absorption measurements in the ultraviolet, visible, and infrared regions and time-resolved photoluminescence experiments were performed. The complex dependence of RL intensity upon rare-earth (RE) concentration and thermal treatment was attributed to the role of OH vibrations as nonradiative recombination channels, as well as to the formation of RE aggregates in the silica matrix. Specifically, the segregation of $CeO_2$ nanoparticles, in which $Ce^{4+}$ does not supply any radiative emission, has been revealed by infrared absorption measurements, in agreement with previous Raman, transmission electron microscopy, and X-ray diffraction data. Moreover, an optical absorption band, centered at 2.4 eV and whose intensity increases with the square of cerium concentration, was observed and tentatively assigned to an intervalence electron-transfer transition involving $Ce^{3+}-Ce^{4+}$ dimers. Postdensification thermal treatments markedly reduce the intensity of this band and increase RL intensity. The relationship between the 2.4 eV band and the RL properties will be outlined. In particular, the increase in RL intensity will be discussed, mainly as a consequence of microscopic modifications leading to an improvement of the charge-transfer efficiency toward emitting centers.

## Introduction

The optical features of cerium in many crystalline and amorphous matrices were intensively investigated from both experimental and theoretical points of view.[1−5] In fact, the strong dependence of both the energy and the splitting of 5d levels upon the host matrix significantly affects the rare earth (RE) optical response and works as a powerful probe of the host crystal field. Several investigations dealt with the optical absorption and photoluminescence emission (PL)/excitation (PLE) properties of $Ce^{3+}$ ion in amorphous silica, prepared by powder fusion or by the sol−gel method.[6−13] The first 4f−5d transition of $Ce^{3+}$ is located at ∼3.8 eV, while the corresponding emission was found mainly at about 2.7 eV. More complex excitation/emission patterns were revealed depending on sample preparation conditions and thermal treatments. Moreover, the optical absorption pattern of Ce-doped silica also features the charge-transfer transition occurring at 4.8 eV, which is a fingerprint of the $Ce^{4+}$ presence (see for example ref 11).

In addition to the fundamental interest toward the knowledge of cerium energy levels in different matrices, it is worth mentioning that cerium is one of the most frequently employed activators in RE-doped systems to be used as scintillators, due to the fast (decay time less than 100 ns) allowed 5d−4f radiative transition occurring in the +3 oxidation state.[2,14] The interest in scintillating materials is presently increasing, due to the development of several application fields such as high-energy physics, medicine, industrial, and security controls. Besides crystalline systems (like, for example, oxides and fluorides), also Ce-doped

* Corresponding author: e-mail anna.vedda@unimib.it.
† University of Milano−Bicocca.
‡ University of Parma.
§ Institute of Physics.

(1) Reisfeld, R.; Hormodaly, J.; Barnett, B. *Chem. Phys. Lett.* **1972**, *17*, 248.
(2) Blasse, G.; Grabmaier, B. C. *Luminescent Materials*; Springer-Verlag: Berlin, Germany, 1994.
(3) Dorenbos, P. *Phys. Rev. B* **2001**, *64*, 125117.
(4) Dorenbos, P. *Phys. Rev. B* **2002**, *65*, 235110.
(5) Ebendorff-Heidepriem, H.; Ehrt, D. *Opt. Mater.* **2000**, *15*, 7.
(6) Stroud, J. S. *J. Chem. Phys.* **1961**, *35*, 844.
(7) Zhenan, G. *J. Non-Cryst. Solids* **1982**, *52*, 337.
(8) Ishii, Y.; Arai, K.; Namikawa, H.; Tanaka, M.; Negishi, A.; Handa, T. *J. Am. Ceram. Soc.* **1987**, *70* (2), 72.
(9) Malashkevich, G. E.; Poddenezhny, E. N.; Melnihenko, I. M.; Boiko, A. A. *J. Non-Cryst. Solids* **1995**, *188*, 107.
(10) Patra, A.; Kundu, D.; Ganguli, G. *J. Sol-Gel Sci. Technol.* **1997**, *9*, 65.
(11) Reisfeld, R.; Minti, H.; Patra, A.; Ganguli, D.; Gaft, M. *Spectrochim. Acta A* **1998**, *54*, 2143.
(12) Malashkevich, G. E.; Melnihenko, I. M.; Poddenezhny, E. N.; Boiko, A. A. *J. Non-Cryst. Solids* **1999**, *260*, 141.
(13) Reisfeld, R.; Patra, A.; Panczer, G.; Graft, M. *Opt. Mater.* **1999**, *13*, 81.
(14) Rodnyi, P. A. *Physical processes in inorganic scintillators*; CRC Press: Boca Raton, FL, 1997.

10.1021/cm0617541 CCC: $33.50 
Published on Web 12/19/2006

glasses showed promising features in the detection of low-energy radiation.[15−20] In this context, with respect to powder melting, the sol−gel method allows preparation of very high purity glasses at relatively low-temperatures.

Recently, sol−gel-prepared Ce-doped silica-based glasses were considered by the authors as potential scintillating materials, and in a number of studies the xerogel preparation and densification were investigated with the aim of improving the glass optical properties.[21−25] Cerium dispersion in silica was studied and $CeO_2$ nanoparticle segregation for Ce:Si molar ratios above $5 \times 10^{-3}$ was revealed by Raman, X-ray-diffraction (XRD), and transmission electron microscopy (TEM) measurements.[26] Finally, application perspectives were investigated in the field of remote dose monitoring: a radioluminescent (RL) dosimeter, based on a $SiO_2$ optical fiber with the core doped by $Ce^{3+}$ ions as luminescent activators, was developed and tested with promising results.[27,28]

The present investigation is aimed at reaching a more complete picture of the microstructural features affecting the optical properties of Ce in $SiO_2$ matrix. To this purpose, selected sol−gel glasses with Ce content in a wide concentration range and different densification temperatures were studied. The presence of residual OH groups and their role in opening nonradiative recombination channels was carefully considered. Moreover, the possible role played by the silica defect states, both of intrinsic and of extrinsic origin, on the observed optical patterns was discussed. The available literature on this topic is very wide, due to the important role of silica in the photonics technology.[29,30] Finally, the presence of $Ce^{4+}$ ions in the silica matrix, either in isolated or in aggregated form, was considered. The comparison among the results obtained on well-characterized samples by using different experimental techniques like optical absorption in the ultraviolet−visible and infrared (IR) regions, microspectrophotometry, PL, RL, time-resolved PL, and Raman scattering, allowed us to depict the microstructural features governing Ce emission in silica host under ionizing radiation in a careful and coherent way.

## Experimental Section

**Preparation of Glasses.** Silica glasses were prepared by the sol−gel method with tetraethoxysilane (TEOS) and $Ce(NO_3)_3 \cdot 6H_2O$ as precursors. Ce:Si molar ratios ranging from $1 \times 10^{-5}$ up to $5 \times 10^{-2}$ were considered. Undoped samples were also prepared as reference. An ethanol solution of TEOS was mixed under stirring with a suitable amount of $Ce(NO_3)_3 \cdot 6H_2O$ in an ethanol−water solution. TEOS:$H_2O$:EtOH volume ratios were 1:0.6:3. $H_2O$:TEOS molar ratio was 7.4:1. Gelation occurred at 35 °C in a thermostatic chamber in 10−20 days. Transparent monolithic xerogels were obtained by slowly drying the alcogel (7−15 days at 35 °C). Xerogels were successively densified to glasses by thermal treatment at different temperatures $T_d$ (450, 750, 850, 950, and 1050 °C). No significant differences in sample properties were observed by performing the densification processes under a flowing oxygen or an inert ($N_2$ or Ar) atmosphere. For a few samples, densification under reducing (Ar−2% $H_2$) atmosphere was performed. In this case, the final glasses were characterized by stronger $Ce^{3+}$ PL emission but by comparable RL intensity with respect to samples densified in oxidizing or inert atmosphere. Moreover, the RL signal was not reproducible, since it increased along repeated X-ray irradiations, possibly due to the sensitization of luminescent defects or to modifications of cerium valence under reducing conditions. Thus, the present work was directed to understand the structural and optical properties of samples densified under oxidizing or inert atmosphere, which display high reproducibility and radiation hardness, so that they possess more interesting applicative perspectives as scintillator materials. The glass samples were discs of approximately 2 cm diameter and 1 mm thickness. After densification, their density was 2.2 g/cm$^3$.

On several samples, further postdensification rapid thermal treatment (RTT) was performed by use of an oxidizing oxygen−hydrogen flame. Such a treatment typically features a very quick temperature increase (2−4 s) up to 1500−1800 °C, during which the sample is kept for approximately 10 s before rapid cooling in air. The temperature was monitored by an optical pyrometer (Impac IE 120) working at 5140 nm emission.

**Spectroscopic Measurements.** Room-temperature RL measurements were performed on a homemade apparatus featuring a charge-coupled device (CCD) (Jobin-Yvon Spectrum One 3000) coupled to a monochromator operating in the 210−780 nm range as detection system. RL excitation was obtained by X-irradiation through a Be window, using a Philips 2274 X-ray tube with tungsten target operated at 20 kV. During the measurements the sample area was limited to a disk with diameter of 5 mm, to allow absolute comparison between samples of slightly different surface areas. The data were corrected for the spectral response of the detection system. PL and PLE spectra were collected at room-temperature with a homemade setup with a Xe lamp (nearly monochromatic radiation of 1 nm bandwidth was selected) as excitation source and a cooled CCD coupled to a 190 mm spectrograph (10 nm bandwidth) for

(15) Zanella, G.; Zannoni, R.; Dall'lgna, R.; Locardi, B.; Polato, P.; Bettinelli, M.; Marigoet, A. *Nucl. Instrum. Methods Phys. Res., Sect. A* **1994**, *345*, 198.
(16) Zanella, G.; Zannoni, R.; Dall'Igna, R.; Polato, P.; Bettinelli, M. *Nucl. Instrum. Methods Phys. Res., Sect. A* **1995**, *359*, 547.
(17) Auffray, E.; et al. *Nucl. Instrum. Methods Phys. Res., Sect. A* **1996**, *380*, 524.
(18) Weiping, C.; Ye, Z.; Lide, Z. *J. Phys.: Condens. Matter* **1998**, *10*, L473.
(19) Baccaro, S.; et al. *J. Lumin.* **2000**, *87−89*, 673.
(20) Nikl, M.; Nitsch, K.; Mihokova, E.; Solovieva, N.; Mares, J. A.; Fabeni, P.; Pazzi, G. P.; Martini, M.; Vedda, A.; Baccaro, S. *Appl. Phys. Lett.* **2000**, *77*, 2159.
(21) Chiodini, N.; Fasoli, M.; Martini, M.; Rosetta, E.; Spinolo, G.; Vedda, A.; Nikl, M.; Solovieva, N.; Baraldi, A.; Capelletti, R. *Appl. Phys. Lett.* **2002**, *81*, 4374.
(22) Baraldi, A.; Capelletti, R.; Chiodini, N.; Mora, C.; Scotti, R.; Uccellini, E.; Vedda, A. *Nucl. Instrum. Methods Phys. Res., Sect. A* **2002**, *486*, 408.
(23) Vedda, A.; Baraldi, A.; Canevali, C.; Capelletti, R.; Chiodini, N.; Francini, R.; Martini, M.; Morazzoni, F.; Nikl, M.; Scotti, R.; Spinolo, G. *Nucl. Instrum. Methods Phys. Res., Sect. A* **2002**, *486*, 259.
(24) Vedda, A.; Chiodini, N.; Di Martino, D.; Fasoli, M.; Martini, M.; Moretti, F.; Rosetta, E.; Spinolo, G.; Nikl, M.; Solovieva, N.; Baraldi, A.; Capelletti, R. J. *Non-Cryst. Solids* **2004**, *345&346*, 338.
(25) Vedda, A.; Chiodini, N.; Di Martino, D.; Fasoli, M.; Griguta, L.; Moretti, F.; Rosetta, E. *J. Non-Cryst. Solids* **2005**, *351*, 3699.
(26) Di Martino, D.; Vedda, A.; Angella, G.; Catti, M.; Cazzini, E.; Chiodini, N.; Morazzoni, F.; Scotti, R.; Spinolo, G. *Chem. Mater.* **2004**, *16*, 3352.
(27) Vedda, A.; Chiodini, N.; Di Martino, D.; Fasoli, M.; Keffer, S.; Lauria, A.; Martini, M.; Moretti, F.; Spinolo, G.; Nikl, M.; Solovieva, N.; Brambilla, G. *Appl. Phys. Lett.* **2004**, *85*, 6536.
(28) Mones, E.; Veronese, I.; Moretti, F.; Fasoli, M.; Loi, G.; Negri, E.; Brambilla, M.; Chiodini, N.; Brambilla, G.; Vedda, A. *Nucl. Instrum. Methods Phys. Res., Sect. A* **2006**, *562*, 449.
(29) Skuja, L. *J. Non-Cryst. Solids* **1998**, *239*, 16.
(30) Defects in $SiO_2$ and Related Dielectrics: Science and Technology, Erice, Italy, April 8−20, 2000; Proceedings of the NATO Advanced Study Institute; Pacchioni, G., Skuja, L., Griscom, D. L., Eds.; Kluwer Academic Publishers: Dordrecht, The Netherlands, 2000.

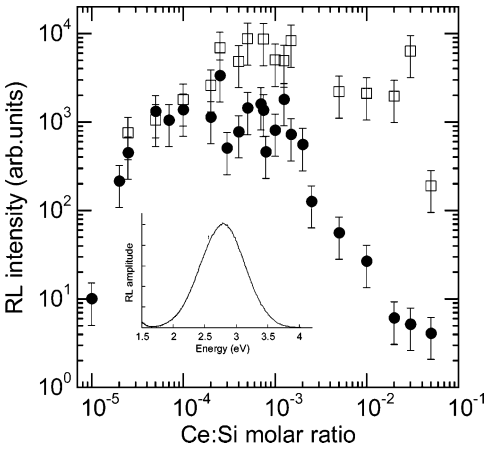


**Figure 1.** Room-temperature RL intensity versus cerium concentration: (●) samples densified at 1050 °C; (□) samples subjected to a postdensification RTT. (Inset) RL spectrum of $5 \times 10^{-4}$ Ce:Si molar ratio as an example.

the signal detection. All the spectra were carefully corrected for the instrumental spectral response. Room-temperature PL time decay measurements were performed by time-correlated single photon counting (TCSPC) with a spectrofluorometer (199S, Edinburgh Instruments) equipped with a pulsed nitrogen flash-lamp; the data deconvolution was performed by the Spectra Solve 4.1 program (Lastex PTY Ltd.). To measure the IR spectra in the high absorption region, chips of glass samples (or of $CeO_2$ powders) were finely ground and mixed with KBr (or CsI) powders in the weight ratio 2:100. Pellets were then prepared from the mixed powders. $CeO_2$ (99.999% purity) powders purchased from Sigma−Aldrich were also used for comparison. IR absorption spectra were measured, as a rule at room-temperature, by means of a BOMEM DA8 Fourier Transform infrared (FTIR) spectrometer in the wavenumber range 200−10 000 $cm^{-1}$. A few spectra were recorded at 9 K, by placing the sample in a 21SC model Cryodine cryocooler of CTI-Cryogenics. Maps of the OH concentration distribution in the samples were obtained by coupling the BOMEM DA8 spectrometer to a Spectra-Tech IR-PLAN microscope. Room-temperature optical absorption measurements in the 1100−185 nm wavelength range were performed by a Varian Cary 50 spectrophotometer. Raman spectra were obtained at room-temperature by using a Dilor micro-Raman spectrometer (excitation by a He−Ne laser at 632.8 nm).

## Results

**Radioluminescence.** The RL intensities, obtained by integration of the RL spectra amplitudes, are reported in Figure 1 for all samples densified at 1050 °C, before and after RTT. The data are mean values of measurements performed on different samples; error bars are also reported. We notice that, despite the very wide concentration range, no significant variations in the shape of the RL spectrum were found. The inset shows the RL amplitude of the sample with Ce:Si molar ratio $5 \times 10^{-4}$ as an example, featuring a band peaked at 2.8 eV and ascribed to the $Ce^{3+}$ 5d−4f radiative transition. No evidence of silica defect-related bands was found. A complex dependence of the RL intensity upon Ce concentration was observed, which is also strongly influenced by RTT. In samples densified at 1050 °C, the maximum luminescence efficiency was observed around $(1 \times 10^{-4})$−$(1 \times 10^{-3})$ Ce:Si molar ratio, while a very strong quenching by more than 2 orders of magnitude was observed

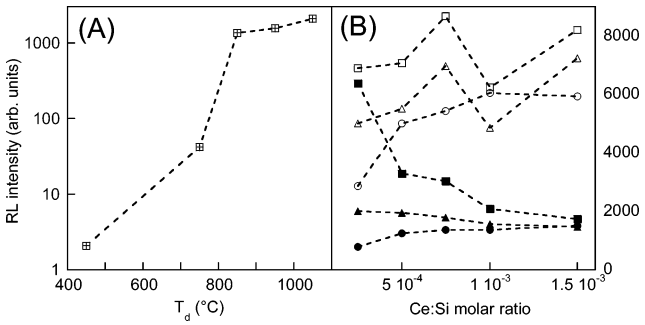


**Figure 2.** (A) Room-temperature RL intensity of $1 \times 10^{-3}$ Ce:Si molar ratio as a function of densification temperature. The dashed line is a guide to the eye. (B) Room-temperature RL intensity of $SiO_2$:Ce as a function of the Ce concentration for different densification temperatures $T_d$: (●) 850, (▲) 950, and (■) 1050 °C. The corresponding open symbols are related to samples subsequently submitted to RTT. Dashed lines are a guide to the eye.

as a consequence of a further increasing of Ce:Si molar ratio up to $5 \times 10^{-2}$. In samples after RTT, the maximum RL intensity was reached approximately in the same range from $1 \times 10^{-4}$ to $1 \times 10^{-3}$ Ce:Si molar ratio; however, its absolute value was higher with respect to samples densified at 1050 °C (roughly by a factor of 5); moreover, luminescence quenching at higher concentrations was by far less pronounced. The densification at 1050 °C was chosen for this RL versus Ce concentration study, since it gave rise to well densified glasses, featuring the highest RL intensity with respect to samples densified at lower temperatures.[23] In Figure 2A, for completeness we report the strong increase of RL intensity versus $T_d$ in a representative case, that of $1 \times 10^{-3}$ Ce:Si molar ratio. In addition, we considered a sample set with Ce:Si molar ratio varying in the interval from $2.5 \times 10^{-4}$ to $1.5 \times 10^{-3}$ (the range in which maximum RL is detected) and with different densification temperatures close to those for optimum densification, namely 850, 950, and 1050 °C. The results are reported in Figure 2B, where the combined effects of densification temperature and Ce concentration are portrayed. Interesting results were obtained, especially prior to RTT (solid symbols): the largest differences among various $T_d$ were observed at the lowest concentrations, while very close data were obtained at the highest value of Ce:Si molar ratio of $1.5 \times 10^{-3}$. Moreover, a slight RL increase upon increasing Ce concentration was observed in samples densified at 850 °C, while an opposite trend was detected in those at 950 °C, which became very pronounced in those at $T_d = 1050$ °C, as also reported in Figure 1. When RTT is performed after densification (open symbols), RL intensities clearly increase for all $T_d$ in accordance with the results displayed in Figure 1.

**FTIR Absorption Measurements.** FTIR spectroscopy was applied to detect (1) the vibrational spectra of OH groups, as belonging either to residual $H_2O$ or to silanol (Si−OH); (2) the $Ce^{3+}$ $^2F_{5/2} \rightarrow {}^2F_{7/2}$ crystal field transition; (3) the possible shift of the intrinsic Si−O−Si overtone stretching mode, as a consequence of the rapid thermal treatment; and (4) the presence of segregated $CeO_2$ phase (see the section Evidence of Ce-Related Clusters).

The presence of OH in samples was monitored by the absorption bands attributed to the Si−OH stretching mode at ∼3670 $cm^{-1}$ [22] and to Si−OH combination mode (stretch-

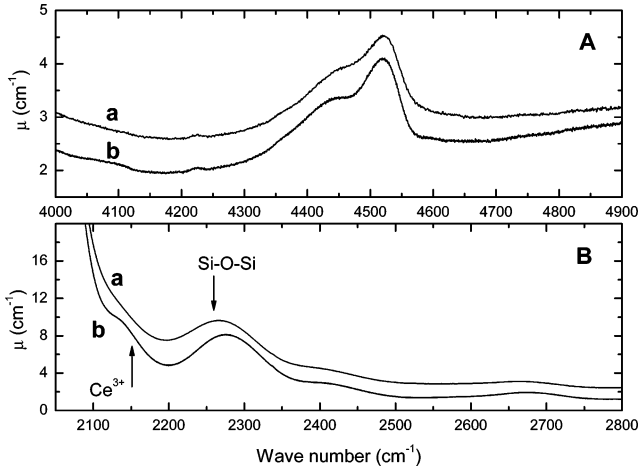


**Figure 3.** Absorption spectra of a $5 \times 10^{-2}$ Ce:Si molar ratio sample ($T_d$ = 1050 °C). (A) Si−OH combination (stretching + bending) mode absorption spectra measured at room-temperature (curve a) and at 9 K (curve b). (B) $Ce^{3+}$ crystal field and overtone of the Si−O−Si stretching absorption spectra measured at room-temperature (curve a) and at 9 K (curve b).

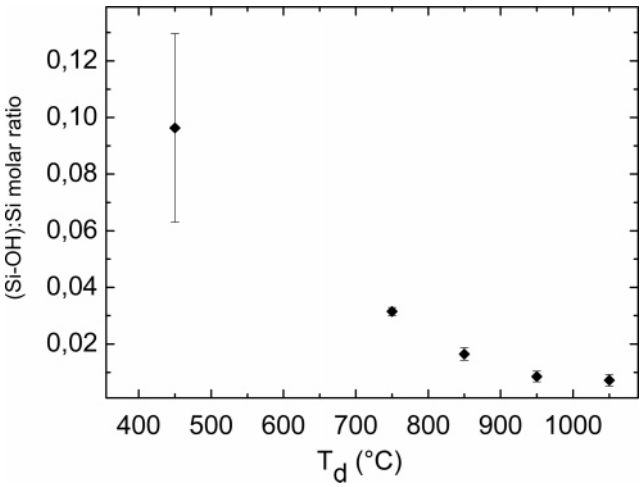


**Figure 4.** Si−OH concentration (mean value) as a function of the densification temperature $T_d$ for samples doped with different Ce concentrations (see text for details).

ing + bending) at ∼4520 $cm^{-1}$, shown in Figure 3A. The shape of the two bands in Ce-doped glasses, as measured at room-temperature, did not show any meaningful difference from that monitored in undoped samples, notwithstanding the wide Ce concentration range (from $1 \times 10^{-5}$ to $5 \times 10^{-2}$). Low-temperature (9 K) spectra did not reveal any additional feature even in the samples with the highest Ce amount (compare curves a and b in Figure 3A). The Si−OH concentration ($C_{OH}$) was evaluated by following the calibration procedures proposed for fused silica[31] and based on the measurement of either the peak amplitude or the area subtended by the above-mentioned absorption bands at 3670 and 4520 $cm^{-1}$, respectively. $C_{OH}$ was found to depend on the densification temperature $T_d$ and on the sample thickness $d$. It decreases with increasing $T_d$ as shown in Figure 4, where $C_{OH}$ is plotted as a function of $T_d$. The IR spectra of samples densified at 450 and 750 °C showed a still large amount of water (peak at about 3500 $cm^{-1}$) in addition to a large Si−OH content.[22] For $T_d \geq 850$ °C, water is no longer

(31) Davis, K. M.; Agarwal, A.; Tomozawa, M.; Hirao, K. *J. Non-Cryst. Solids* **1996**, *203*, 27.

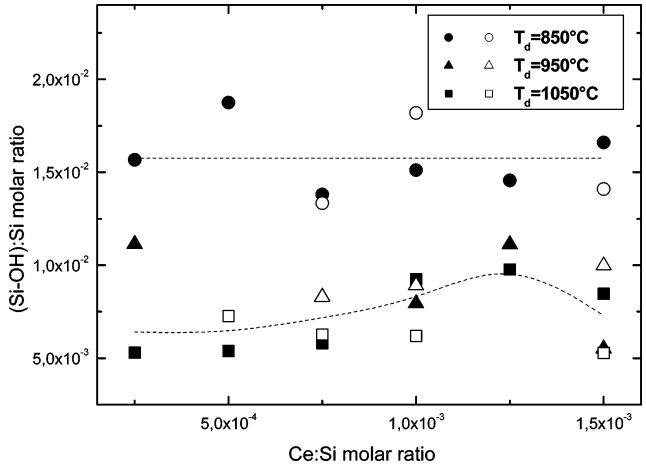


**Figure 5.** Si−OH concentration as a function of the Ce concentration for different densification temperatures $T_d$: (●) 850, (▲) 950, and (■) 1050 °C. The corresponding open symbols are related to samples subsequently submitted to RTT. The dashed lines are guides to the eye.

detected and $C_{OH}$ decreases smoothly, attaining a saturation value for temperatures higher than 1000 °C. In fact, even an RTT, during which temperatures as high as 1800 °C are reached, does not succeed in producing further reduction of $C_{OH}$. The detailed behavior of $C_{OH}$ versus Ce concentration is reported in Figure 5 for the above samples densified at $T_d$ = 850, 950, and 1050 °C and for those that were submitted to RTT. At variance with the RL results (see Figure 2), there is no evident dependence of the Si−OH content on the Ce concentration, at least for Ce:Si molar ratios from $2.5 \times 10^{-4}$ to $1.5 \times 10^{-3}$. The spread of the data may be related to the different thicknesses of the samples measured. In fact, for fixed Ce amount and $T_d$ = 1050 °C, the Si−OH concentration was found to increase by increasing the sample thickness $d$. FTIR microspectrophotometric analysis showed that the Si−OH concentration profile along the sample thickness is nearly flat in thin (i.e., $d$ = 0.6 mm) samples, while in thicker samples (i.e., 1.2 mm) it exhibits a plateau in the middle, accompanied by an appreciable decrease on both sides. This means that the water molecules, and as a consequence OH groups, leave the sample through a diffusion process. The results reported in Figure 5 and referred to samples submitted to RTT (open symbols) show that the treatment does not modify the Si−OH content significantly, even in samples previously densified at rather low-temperatures, as 850 and 950 °C. By summarizing the results obtained on about 70 different well densified samples (i.e., $T_d$ = 1050 °C), and for Ce:Si ratio in the range $(0-5) \times 10^{-2}$, the (Si−OH):Si molar ratio was found to range between $5 \times 10^{-3}$ and $2 \times 10^{-2}$.

The presence of $Ce^{3+}$ was assessed by a weak shoulder at about 2150 $cm^{-1}$ overlapped to the intrinsic vibrational absorption of silica; see Figure 3B (curve a). Its amplitude increased by increasing the nominal Ce concentration. The shoulder became more pronounced by measuring the spectra at low-temperature (9 K), but remained in any case broad as expected for a crystal field transition ($^2F_{5/2} \rightarrow {}^2F_{7/2}$) of $Ce^{3+}$ embedded in the disordered silica matrix (compare curves a and b in Figure 3B).

The broad peak appearing at about 2260 $cm^{-1}$ in pure and Ce-doped samples ($T_d$ = 1050 °C), see curve a in Figure

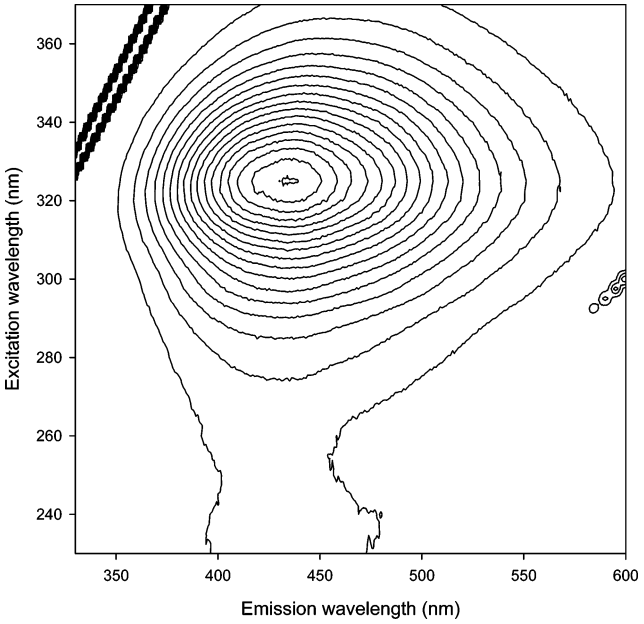


**Figure 6.** Contour plot of the room-temperature PL excitation−emission pattern of $1 \times 10^{-4}$ Ce:Si molar ratio ($T_d = 1050$ °C).

3B, is attributed to an overtone of the Si−O−Si fundamental stretching mode peaking at about 1100 $cm^{-1}$. Both bands were found to be related in fused silica samples to the so-called fictive temperature and shift to lower frequencies with the decrease of the average Si−O−Si bond angle in the glass structure: the shift is associated to a densification of the glass matrix.[32] In the present silica samples, prepared via sol−gel and densified at 1050 °C, the position of the overtone is comparable to that reported for the fused silica and shifts to shorter wavenumbers (about 10 $cm^{-1}$) when samples are submitted to RTT. This means that a further rearrangement of the Si−O−Si bonds may take place as a consequence of RTT.

**Steady-State and Time-Resolved Photoluminescence.** PL measurements were performed in order to put in evidence energy transfer phenomena possibly responsible for the observed quenching of the $Ce^{3+}$ emission. First of all, the contour plot of the excitation−emission pattern is reported in Figure 6 in the case of Ce:Si molar ratio $1 \times 10^{-2}$, with $T_d = 1050$ °C. The emission band is similar to that detected by RL measurements; it features an excitation spectrum peaking at 325 nm (3.81 eV), corresponding to the lowest 4f−5d transition of $Ce^{3+}$ in $SiO_2$ host.[6−13] Detailed time-resolved PL measurements were performed on several samples, densified at 1050 °C, before and after RTT, by exciting at 3.94 eV and monitoring the emission at 2.95 eV. Nonexponential decays, in the $10^{-8}$−$10^{-7}$ s time scale, were observed in all cases. Examples of PL decays are reported in Figure 7 in the case of Ce:Si molar ratio $4 \times 10^{-4}$ before and after RTT: a slightly more pronounced decay distortion is evident before RTT. The numerical analysis of PL decay measurements was carried on by data deconvolution in terms of two exponential decays plus the excitation pulse. The choice of two exponentials was determined by the evident nonexponential character displayed by the curves in Figure

(32) Agarwal, A.; Davis, K. M.; Tomozawa, M. *J. Non-Cryst. Solids* **1995**, *185*, 191.

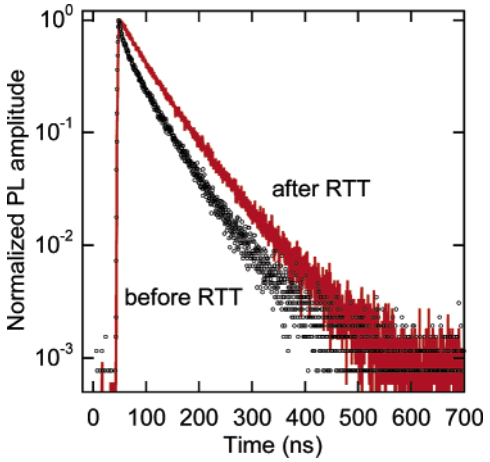


**Figure 7.** Normalized PL time decays of $4 \times 10^{-4}$ Ce:Si molar ratio ($T_d = 1050$ °C), before and after RTT obtained at room-temperature. $E_{exc} = 3.94$ eV, $E_{em} = 2.95$ eV.

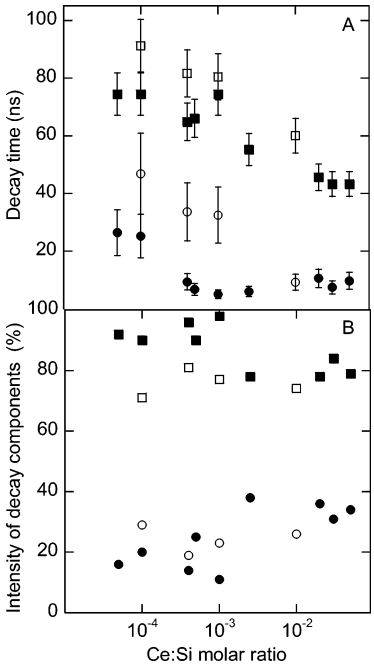


**Figure 8.** (A) Decay times ($\tau$) of $SiO_2$:Ce versus Ce concentration obtained from deconvolution of room-temperature PL decays with the sum of two exponential components. (●) $\tau_1$ and (■) $\tau_2$ of $SiO_2$:Ce after densification at 1050 °C; (○) $\tau_1$ and (□) $\tau_2$ of $SiO_2$:Ce after RTT are shown. $E_{exc} = 3.94$ eV, $E_{em} = 2.95$ eV. (B) Intensities of decay components of $SiO_2$:Ce versus Ce concentration obtained from deconvolution of room-temperature PL decays in terms of two exponentials. Intensities of the (●) short ($\tau_1$) and (■) long ($\tau_2$) components of $SiO_2$:Ce after densification at 1050 °C and of the (○) short ($\tau_1$) and (□) long ($\tau_2$) components of $SiO_2$:Ce after RTT are shown. $E_{exc} = 3.94$ eV; $E_{em} = 2.95$ eV.

7 and succeeded in accounting for them satisfactorily in all cases. The so-obtained decay times ($\tau_1$ and $\tau_2$) are reported in Figure 8A, where the solid symbols refer to samples densified at 1050 °C and the open symbols to samples subjected to RTT. Both $\tau_1$ and $\tau_2$ decay times shorten by increasing Ce concentration. Slightly higher decay time values were obtained after RTT. On the contrary, their relative weights do not significantly vary, as displayed in Figure 8B. We are aware that the two-exponential fit is just a mathematical data reconstruction, and care must be taken when its physical meaning is considered. In our case, at least two factors contributing to the decay nonexponential character might be mentioned. Due to the amorphous structure

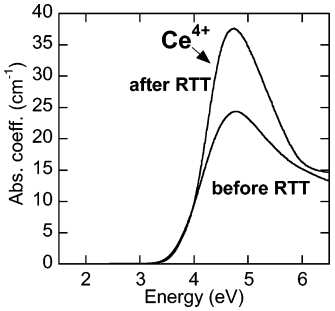


**Figure 9.** Room-temperature optical absorption spectrum of $1 \times 10^{-3}$ Ce:Si molar ratio ($T_d$ = 950 °C).

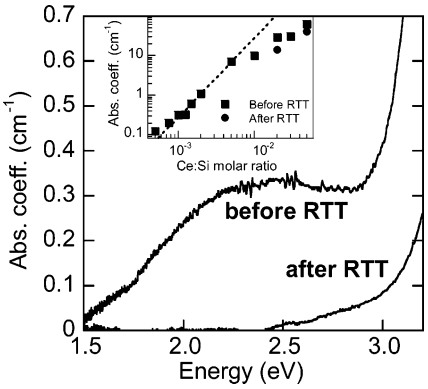


**Figure 10.** Room-temperature optical absorption spectra in the 1.5−3.2 eV energy region of $1 \times 10^{-3}$ Ce:Si molar ratio densified at 1050 °C before and after RTT. (Inset) Intensity of the 2.4 eV absorption band as a function of cerium concentration (■) before RTT and (●) after RTT. Dashed continuous line represents a quadratic function.

of the host, it is possible that isolated $Ce^{3+}$ is incorporated in slightly different environments, leading to a distribution of decay times and to a distorted decay, which is satisfactorily deconvolved in terms of two exponentials. In addition, the shortening of such decay times as a consequence of Ce concentration increase suggests either energy transfer phenomena toward defects or luminescence quenching in the presence of aggregates, as will be discussed in the following sections.

**Visible and UV Optical Absorption Measurements.** The room-temperature optical absorption spectrum of Ce-doped silica is dominated by a band at 4.8 eV: this is a fingerprint of the presence of $Ce^{4+}$, being related to a charge-transfer transition. The intensity of this band (and hence the concentration of $Ce^{4+}$) rapidly increases with increasing cerium concentration and $T_d$. It could be correctly measured only at Ce:Si molar ratio $1 \times 10^{-3}$. Figure 9 displays the spectra obtained on samples with Ce:Si molar ratio $1 \times 10^{-3}$ densified at 950 °C, before and after RTT, and shows that the latter process causes an increase of $Ce^{4+}$ ions too (the oxidizing oxygen−hydrogen flame employed for RTT might be responsible for $Ce^{3+}$ oxidation; see Experimental Section). At lower energies, the spectra reveal a defect-related band at 2.4 eV, which increases with cerium amount (Figure 10) and is responsible for the blue-violet glass coloration, which is evident for Ce:Si molar ratios higher than $5 \times 10^{-3}$. This band, and consequently glass coloration, is fully suppressed by RTT, at least up to a Ce:Si molar ratio of about $1 \times 10^{-2}$. At higher Ce concentrations, RTT reduces its intensity by a factor of 2−3. A detailed investigation of the band

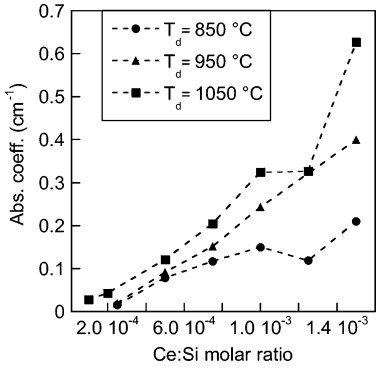


**Figure 11.** Intensity of the 2.4 eV optical absorption band versus cerium concentration: samples densified at $T_d$ = (●) 850, (▲) 950, and (■) 1050 °C are shown. Dashed lines are a guide to the eye.

intensity performed on the same sample set, whose RL data are considered in Figure 2, is reported in Figure 11, which confirms its rapid increase upon $T_d$ and Ce concentration increase. It is interesting to remark that, in the Ce:Si molar ratio range from $5 \times 10^{-4}$ to $5 \times 10^{-3}$, the band intensity depends on the square of Ce amount: a straight line of slope 2 fits well the experimental data in the log−log plot displayed in the inset of Figure 10.

**Evidence of Ce-Related Clusters: Raman and FTIR Measurements.** The formation of Ce-containing aggregates may seriously affect the activator luminescence. Actually, an extensive investigation on the presence and properties of $CeO_2$ particles in Ce-doped sol−gel silica glasses was recently performed by us using Raman, XRD, and TEM measurements.[26] In the present paper, we summarize such results to provide, with a comprehensive description of all factors influencing luminescence, a background for a sound discussion. From an experimental point of view we add here the identification of $CeO_2$ aggregates, as monitored by infrared absorption measurements. The Raman spectra of samples with Ce:Si molar ratio $5 \times 10^{-2}$ before and after RTT, compared to the Raman spectrum of $CeO_2$ powders, are reported in Figure 2 of ref 26. The presence of $CeO_2$ nanoparticles is revealed by the Raman structure peaking at 460 $cm^{-1}$ and assigned to the symmetric stretching vibration of $CeO_2$.[33] Actually, the presence of such particles was unveiled only in samples with Ce:Si molar ratios higher than $5 \times 10^{-3}$. In samples submitted to RTT, Raman peak position slightly shifted to higher wavenumbers, while the peak width decreased with respect to that in the same glasses before RTT, suggesting that RTT induces an increase of the $CeO_2$ nanocrystal size. The $CeO_2$ nanocrystal diameter was evaluated by XRD measurements on samples subjected to RTT, versus cerium concentration. The aggregate diameters, ranging from 15 nm (for Ce:Si molar ratio $10^{-2}$) up to 20 nm (for Ce:Si molar ratio $5 \times 10^{-2}$), were also confirmed by TEM measurements.[26]

A further support to the presence of $CeO_2$-separated phase is provided by the FTIR spectra of pellets (see Experimental Section) in the wavenumber range 200−700 $cm^{-1}$, displayed in Figure 12. These are related to a silica sample with Ce:Si molar ratio $5 \times 10^{-2}$ (curve a), a pure silica sample (curve

(33) Weber, W. H.; Hass, K. C.; Mc Bride, J. R. *Phys. Rev. B* **1993**, *48*, 178.

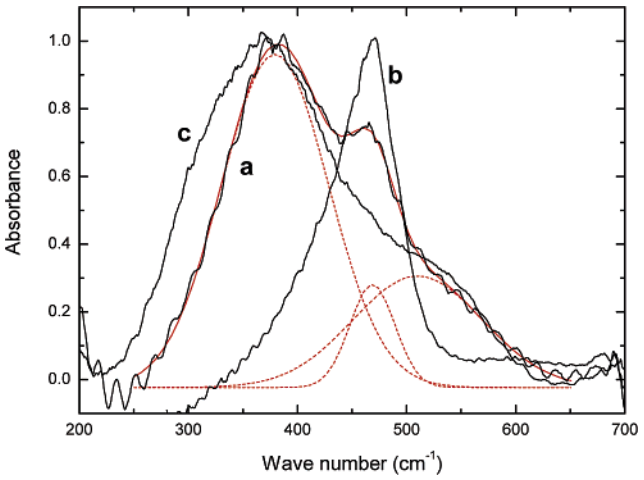


**Figure 12.** Comparison among the FTIR absorption spectra of $5 \times 10^{-2}$ Ce:Si molar ratio (curve a), undoped $SiO_2$ (curve b), and $CeO_2$ (curve c) in the low-wavenumber range (glass samples densified at $T_d = 1050$ °C). The measurements were performed at room-temperature on pellets obtained by mixing undoped $SiO_2$ with KBr powders, $5 \times 10^{-2}$ Ce:Si molar ratio, and $CeO_2$ with CsI powders, in weight ratio 2:100. The dashed red curves represent the Gaussian components contributing to curve a. Their sum is portrayed by the thin red line.

b), and $CeO_2$ powders (curve c). The spectrum of the heavily Ce-doped silica shows a peak at about 468 cm$^{-1}$, which coincides with that of the pure silica sample (compare curves a and b) and is attributed to the rocking vibration of the Si−O−Si bridges.[32] In addition, two broader bands appear at about 379 and 510 cm$^{-1}$. Their positions are in good agreement with those of the bands displayed by $CeO_2$ pellet (compare curves a and c), that is, 367 and 507 cm$^{-1}$, respectively, as derived by a fitting of the curves in terms of Gaussians. This analysis has the unique purpose to stress the similarity of the spectra related to the two pellets containing chips of Ce-doped silica and $CeO_2$ microcrystalline powders, respectively. No specific physical meaning is attributed to the frequencies at which the Gaussians are peaking. In fact, the spectra we are measuring should be regarded as reflectivity spectra rather than absorption ones, since the measurements are performed in the $CeO_2$ reststrahlen ("residual radiation") region, which ranges from the transverse optical (TO) frequency (272 cm$^{-1}$) to the longitudinal optical (LO) one (595 cm$^{-1}$) and is characterized by very high reflectivity (about 87% in $CeO_2$ single crystals).[33,34]

## Discussion and Conclusions

The complex dependence of Ce-related radioluminescence intensity upon Ce concentration and $T_d$ displayed in Figures 1 and 2 demonstrates that several factors affect the optical properties of this activator in silica. They are related to the structural properties of the host matrix, strongly depending upon preparation conditions, and to luminescence features mostly connected to microscopic mechanisms switched on by the activator incorporation. As far as the host matrix is specifically concerned, the most important aspect to consider is the presence of OH groups. It is well-known that the OH-related vibrations quench radiative emission,[2] hence the presence of either residual water or Si−OH groups should be avoided in a scintillator material. High amounts of water are present in the xerogels,[22] so that the glass densification process is recognized as a key step to obtain a stable matrix with the minimum concentration of OH groups. The comparison between RL intensity (Figure 2A) and Si−OH concentration (Figure 4) versus $T_d$ well reflects the effectiveness of Si−OH removal in improving the material luminescence efficiency. The same mechanism is also responsible for the high RL signal observed in Figure 2B in the low Ce concentration range for $T_d = 1050$ °C and before RTT, although the decrease of OH groups, at least in the 850−1050 °C range, is limited (see Figure 4). However, in the same Figure 2B it is evident that, as far as Ce concentration increases, the role of OH concentration becomes less pronounced and other factors limiting the luminescence efficiency start to dominate. These are the same factors that modulate the complete RL versus Ce concentration trend in Figure 1. The existence of other mechanisms is also clearly demonstrated by the distinct behavior of Si−OH concentration and RL intensity, as a consequence of RTT (compare Figures 2B and 5). Such a treatment has no effect on Si−OH concentration; in fact, a decrease of Si−OH groups is accomplished through the diffusion process of OH from the bulk to the surface (long-distance migration), as suggested by microspectrophotometry measurements (see the section FTIR Absorption Measurements). It would require, for a significant OH removal, times longer than 10 s, even at high temperatures (see Experimental Section). On the contrary, other processes, as for example $Ce^{3+}-Ce^{4+}$ dimer oxidation or dissociation, may be accomplished even in short times. Thus RTT may cause strong RL enhancement; see Figures 1 and 2B.

Therefore, Ce aggregation phenomena as important sources of luminescence quenching at elevated Ce concentration should be taken into account. In this respect the experimental evidence of $CeO_2$ aggregate formation might play a key role. The existence of a $CeO_2$ separate phase was recently confirmed by parallel XRD, TEM, and Raman measurements[26] and, in the present paper, also by IR data (see the section Evidence of Ce-Related Clusters). The experimental evidence was obtained at Ce:Si molar ratios higher than $5 \times 10^{-3}$, although, when the sensitivity limits of the techniques used are taken into account, the cluster formation might start at still lower concentrations. Furthermore, the strong charge transfer absorption band at 4.8 eV (Figure 9) assesses the presence of $Ce^{4+}$ (although not necessarily in the form of $CeO_2$ clusters), even at low Ce concentrations. At variance with $Ce^{3+}$, $Ce^{4+}$ does not contribute to luminescence: the occurrence of the activator as a tetravalent cation is useless for scintillating applications, independently of the form under which it is present in the matrix (as a dispersed ion or in $CeO_2$ aggregates). It was also noted that RTT causes an increase of $CeO_2$ cluster size:[26] so, the strong RL increase observed following RTT treatment remains unexplained if only $CeO_2$ segregation is considered.

Looking for different mechanisms responsible for the strong RL increase following the RTT, we observe that an interesting feature is the occurrence, at high Ce concentrations and with increasing $T_d$, of an optical absorption band

(34) Marabelli, F.; Wachter, P. *Phys. Rev. B* **1987**, *36*, 1238.

centered at 2.4 eV (see Figures 10 and 11). In general, and independently of its microscopic nature, the presence of an absorption band in the visible spectral region, partly overlapping with $Ce^{3+}$ emission, is a detrimental feature in a material to be used as scintillator, since it causes reabsorption of the emitted light. Interestingly, the RTT causes the complete disappearance of such an absorption in samples with cerium contents up to Ce:Si molar ratios $\approx 1 \times 10^{-2}$.

A band in a similar spectral region was detected in pure $SiO_2$ and attributed to nonbridging oxygen hole centers (NBOHC).[29] Optical excitation of NBOHC should give rise to the characteristic emission centered at 1.9 eV. We failed to detect any PL emission by exciting our samples at 2.4 eV, in spite of several attempts performed by using a tungsten halogen lamp as well as a He−Ne laser source. Alternatively, the observed band might be due to a Ce-related defect, as explicitly suggested by its increase in intensity when Ce concentration increases. In fact, in the literature an assignment concerning this band was made as possibly due to $Ce^{3+}$−oxygen complexes having $Ce^{4+}$ ions in their nearest surroundings.[9] Although the detailed structure of this center can hardly be identified, our data, showing a quadratic dependence of the 2.4 eV band amplitude upon cerium concentration (inset, Figure 10), suggest the hypothesis of defect complexes containing $Ce^{3+}$−$Ce^{4+}$ dimers giving rise to an intervalence electron-transfer transition to which the 2.4 eV absorption band could be associated.[35] In a simple thermodynamic defect equilibrium approach, the ratio between the concentration of pairs of Ce ions $\chi_p$ and that of isolated ions $\chi$ can be written as[36]

$$\chi_p/\chi^2 = a \exp(\Delta g^p/kT) \qquad (1)$$

where $a$ is a constant depending on the number of distinguishable orientations of the pair, $\Delta g^p$ is the free energy released when the two isolated ions form the pair, and $k$ is the Boltzmann constant. In eq 1 the concentration of isolated ions can be considered roughly proportional to the nominal cerium doping in the limit of a very low pair concentration. It well describes our data in the range of Ce:Si molar ratios from $5 \times 10^{-4}$ to $5 \times 10^{-3}$. At higher concentrations, also other competing phenomena like $CeO_2$ large particle formation start to occur, and thus a departure from the quadratic law is observed. The disappearance of $Ce^{3+}$−$Ce^{4+}$ pairs following RTT, at least up to Ce:Si molar ratio $\approx 1 \times 10^{-2}$, is correlated with the increase of luminescence efficiency depicted in Figure 1. In this way, an improvement of the overall transparency of the material to the light emitted by $Ce^{3+}$ ions is obtained. After RTT, the RL is dominated by the emission of well-isolated $Ce^{3+}$ ions, as confirmed by the PL time-resolved measurements, since samples subjected to RTT display less distorted and slightly longer time decay profiles (Figures 7 and 8A).

However, the disappearance of the 2.4 eV absorption band is probably not the only factor responsible for the RL increase after RTT in the lowest Ce:Si molar ratio range (from $1 \times 10^{-4}$ to $1 \times 10^{-3}$), due to its weak intensity prior to the thermal treatment (see Figure 10). Moreover, we remark that recent RL experiments performed on $SiO_2$ samples doped with $Gd^{3+}$ revealed that also the $^6P_{7/2}$−$^8S$ $Gd^{3+}$ emission is markedly increased by RTT.[37] Thus, especially in the low Ce concentration regime, the RL increase should be also partly ascribed to microscopic modifications leading to an improvement of the charge-transfer efficiency toward emitting centers independent of the nature of the activator (as well as of the OH content). In this respect it should be taken into account that the RL phenomenon involves recombination of carriers (holes and electrons) previously made free into valence and conduction bands, respectively. Thus, at variance with PL recombination, RL can suffer from additional detrimental processes, such as carrier trapping by defects. Carrier trapping by defects and its influence on spectral and temporal characteristics of scintillators is the subject of several investigations in different materials.[38,39] In sol−gel glasses, the presence of defects acting as traps was documented by recent thermally stimulated luminescence (TSL) studies,[25] which revealed also the common, intrinsic nature of traps in glasses doped with several rare-earth ions, as well as in undoped $SiO_2$ samples of different origin. The correlation between these defects and oxygen vacancies was proposed in several papers (ref 25, and references 9−11 therein). Although the glow curves of Ce-doped silica glasses before and after RTT displayed similar structures, a reduction of a TSL peak at about 550 K was observed after RTT, and this might be considered as an indication that this process causes also the removal of intrinsic point defects that act as trapping channels and compete with the prompt RL emission.

In conclusion, high-efficiency scintillating glasses could be obtained by the sol−gel method. The reproducibility of their scintillation response was assessed by a careful choice of the densification atmosphere, and the optimal Ce doping level was found. The principal microstructural features governing Ce luminescence in silica glass have been identified, like the presence of OH groups, of Ce-related clusters and dimers, as well as the existence of point defects affecting the charge transfer toward emitting centers during the RL process. Therefore, the scintillation efficiency of sol−gel glasses doped by cerium might be further improved by analyzing and then controlling the nature of point defects present in the glass structure. Thus, the setting-up of a modified glass preparation procedure aimed at minimizing the deep trap levels might lead to the removal of an important competitive process for ionized carriers and give rise to a further RL efficiency improvement.

**Acknowledgment.** Financial support of the Fondazione Cariplo in the framework of the project "Structural and optical properties of self-organized nano- and mesoscopic materials" (2005−2007) is gratefully acknowledged.

CM0617541

(35) *The Electronic Structure and Chemistry of Solids*; Cox, P. A., Ed.; Oxford University Press: Oxford, U.K., 1987.
(36) *Point Defects in Solids*; Crawford, J. H., Slifkin, L. M., Eds.; Plenum Press: New York, 1972.
(37) Moretti, F.; Chiodini, N.; Fasoli, M.; Griguta, L.; Vedda A. *J. Lumin.* **2006** (submitted for publication).
(38) Wojtowicz, A. J. *Nucl. Instrum. Methods Phys. Res., Sect. A* **2002**, *486*, 201.
(39) Nikl, M. *Phys. Status Solidi A* **2005**, *202*, 201.